Efficient THz generation by femtosecond laser pulses and using THz radiation for plasma diagnostics

Andrey N. Stepanov [1*], Sergey B. Bodrov [1, 3], Igor E. Ilyakov [1], Aleksey I. Korytin [1], Nickolay L. Aleksandrov [2], and Nickolay V. Vvedenskii [1, 3]

[1] Institute of Applied Physics, Russian Academy of Sciences, Nizhny Novgorod 603950, Russia

[2] Moscow Institute of Physics and Technology, Dolgoprudny 141700, Russia

[3] University of Nizhny Novgorod, Nizhny Novgorod 603950, Russia

[*1] Email: step@ufp.appl.sci-nnov.ru

Abstract: Optical-to-terahertz conversion of femtosecond laser radiation by optical rectification in the $LiNbO_3$ crystal and two-color gas ionization in air is discussed. It is shown that a high energy conversion efficiency (~0.25%) is achieved by Čerenkov radiation of line-focused femtosecond pulses propagated in a sandwich structure with a thin $LiNbO_3$ core covered with a Si prism. The effect of different substrates of the sandwich structure as well as laser pulse duration on the generation efficiency and terahertz spectrum is explored. The tilted pulse front technique for phase-matched THz generation using room-temperature and cryogenically cooled $LiNbO_3$ is studied under conditions of weak and strong laser pump for different crystal lengths and pump pulse durations. It is shown that the optical-to-terahertz conversion efficiency saturates as a result of the Kerr self-phase modulation of the optical pump. Low-frequency THz generation by two-color femtosecond laser pulse ionization of the ambient air is studied both experimentally and theoretically in the case of the main field at the fundamental and a weak additional field tunable near the half-harmonic frequency. The dependences of the THz yield and polarization on the parameters of the two-color pulse are determined. The analytical formulas obtained using the model of the free-electron residual current density give an excellent agreement with the experimental results. For demonstration of the THz radiation application, we use scattering of terahertz radiation to measure the air plasma density decay in a filament produced by an intense femtosecond laser pulse in air. It is shown that the plasma density decreases by about two orders of magnitude within 2 *ns* after the ionization and the rate of plasma decay can be decreased by applying an additional high (several *kV/cm*) external electric field. Numerical simulation of the electron density decay and electron temperature evolution is performed taking into consideration dissociative and three-body electron-ion recombinations as well as the formation of complex positive ions, in good agreement with the experimental data.

Keywords: Efficient terahertz generation, Optical-to-terahertz conversion, Terahertz scattering, Plasma density decay

1. Introduction

Terahertz science develops very quickly the last few decades whether you speak about the

sources of THz radiation, their diagnostics, or various THz applications. The development of lasers producing femtosecond pulses provides a variety of ways for tabletop generation of short (up to one-cycle) terahertz (THz) pulses. Biased photoconductive switches gated by femtosecond laser pulses are commonly used. With a large-area photoconductive emitter, it is possible to create a high THz field (about several tens of *kV/cm*) with a conversion efficiency of about 10^{-3} [1].

Another well-established way of generating broadband terahertz radiation is optical rectification of femtosecond laser pulses in electro-optic crystals. Phase-matched terahertz excitation can be achieved in the ZnTe crystal pump by Ti:Sa laser pulses (~ 800 *nm* wavelength). But due to a strong two-photon pump absorption, the optical-to-terahertz conversion efficiency in this scheme is rather low (typically, 10^{-6}-10^{-4}) [2, 3]. Using a large-aperture ZnTe crystal, 1.5-*μJ* THz pulses were generated [4]. Another promising crystal for optical rectification is $LiNbO_3$ (LN). The nonlinear coefficient of this crystal is ~ 2.5 *times* larger than that of ZnTe [5], and it has a wider bandgap and does not suffer from two-photon absorption when illuminated by a Ti:Sa laser. However, collinear velocity matching is impossible in this material because its terahertz refractive index is more than two times larger than the optical group refractive index. Additionally, $LiNbO_3$ has a strong terahertz absorption at room temperature, namely, $\sim 16-170\ cm^{-1}$ at $1-2.5$ *THz* [5]. To compensate for the velocity mismatch, a periodically poled lithium niobate structure [6, 7] or use of a tilted pump intensity front [8] were proposed. In the first technique, multicycle narrowband terahertz wave packets are generated via a quasi-phase-matched mechanism with efficiency typically below 10^{-5} [6, 9]. The second technique allows phase-matched generation of a wideband (from 0.1 to 2 *THz*) THz pulses with tens of *μJ* pulse energy [10-12], a more than 1 *MV/cm* peak electric field [13], and record values of conversion efficiency ($>10^{-3}$). Strong terahertz absorption in $LiNbO_3$ still remains an essential limitation in this technique. Efficient THz generation can be achieved in the $LiNbO_3$ crystal not only by collinear phase matching, but also by the Čerenkov radiation mechanism [14, 15]. For this, the laser beam should have a size of the order of (or smaller than) the terahertz wavelength (~ 50 *μm* for 1 *THz*). Strong terahertz absorption in $LiNbO_3$ can be minimized by aligning the laser beam in parallel to the lateral surface of the crystal and putting a low terahertz absorbing Si-prism coupler on the surface to output the Čerenkov radiation from the crystal [16].

The high-energy THz generation technique based on mixing of the optical fundamental and the second harmonic in the laser-induced plasma was proposed in [17] and examined in the numerous publications (see, e.g., [18, 19]). THz generation in such a way is inferior in energy to the tilted pulse front approach, but it has a very broad (up to a 100-*THz* bandwidth) spectrum [19, 20], which allows a *MV/cm* peak THz electric field to be generated [21].

In the present paper, we summarize our studies of efficient THz generation with LN crystal using Čerenkov radiation and tilted pulse front techniques, as well as using air ionization by two-

color femtosecond laser pulses. Also, we demonstrate the use of THz pulses for a study of plasma dynamics in a filament.

The paper is organized as follows. In the first part, we discuss THz generation by the Čerenkov radiation mechanism in the sandwich structures containing a thin LiNbO₃ layer, a Si prism for output THz radiation, and different types of substrates [22, 23]. In the second part, we present the results of our research on the THz generation in the LN crystal pumped by femtosecond pulses with tilt intensity front for different pulse energies and durations, crystal lengths, and temperatures [24]. In the third part, we study, both experimentally and theoretically, low-frequency terahertz emission from the ambient air ionized by a two-color femtosecond laser pulse containing, besides the fundamental-frequency main field, a weak additional field tunable near the half-harmonic frequency [25]. In the last part of the paper, based on the terahertz scattering technique we discuss measurements of the plasma density decay in a filament produced by an intense femtosecond laser in air [26, 27].

2. Terahertz generation in a sandwich-structure with LiNbO₃ layer

A sandwich structure with a thin layer of LiNbO₃ (or another nonlinear material), which was used to excite THz waves by optical rectification, and two Si prisms (or a Si prism and a substrate), which were placed on a lateral surface of the layer to output THz waves in vacuum, was proposed in [28, 29]. Efficient terahertz generation by this sandwich structure is a result of the creation of high nonlinear polarization as a source of THz waves due to a high nonlinear coefficient and the possibility of using strong intensity (>100 GW/cm^2) pump in the LN crystal, as well as the creation of a long tail of the Čerenkov radiation due to guiding of the laser pump and low THz absorption in the Si prism. Line focusing of the optical pump provides additional advantages including the creation of a Čerenkov wedge (a beam having nearly a flat phase front), which is more convenient for practical applications compared with the Čerenkov cone produced by the laser pulse focused into a spot, and the possibility of scaling of the terahertz pulse energy by the length of the line. Below we present experimental studies of THz generation in the sandwich structure with a LiNbO₃ layer.
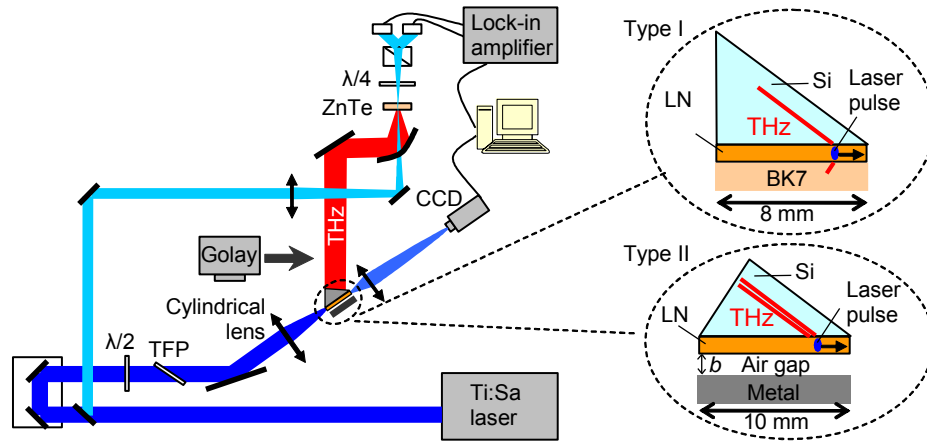
Fig. 1 Experimental setup for THz generation in a sandwich structure.

A schematic of the experiment is shown in Fig. 1. We used two types of the sandwich structures shown on the right-hand side of Fig. 1. In the first, type I structure, a layer of congruent LiNbO$_3$ with thickness a was glued on a BK7 glass substrate and a high-resistivity Si prism with a base angle of 45° was pressed against the upper surface of the LiNbO$_3$ layer. We used two of such structures with a = 30 μm and 50 μm and 8 mm long. In the second, type II structure, a 35 μm thick layer of 1 mol % stoichiometric LiNbO$_3$ 10x10 mm in size was glued on the Si prism, and a metal plate was placed on the opposite side of the LN layer at a precision stage to vary the air gap b between LN and the metal. A commercial Ti:Sa laser (λ=780 nm, 50 fs, 1 kHz, and 2.5 mJ) was used as the optical pump. In the experiment, the pulse energy was varied in the 0-100 μJ range by a polarization attenuator. The laser pulse focused into a line by a cylindrical lens propagated in the LN layer and excited Čerenkov terahertz radiation in the Si prism. In the type I structure, the Čerenkov radiation is also produced in BK7, but it faded rapidly due to the strong THz absorption. In the type II structure, the Čerenkov radiation was absent below the LN layer (only an evanescent terahertz field was present in the air gap). The THz radiation transmitted from the Si prism was measured by a conventional electro-optic sampling technique with the use of a ZnTe crystal. Terahertz energy was measured by a calibrated Golay cell located about 1 cm from the exit facet of the Si prism. Accuracy of the laser beam focusing in the LN layer was monitored by imaging (with x8 magnification) of the optical intensity distribution from the exit facet of the LN layer to a CCD camera by a short-focus lens.

Generated terahertz spectrum for type I and type II sandwich structures are shown in Figs. 2(a) and 2(b), respectively. For both sandwich types, the spectrum is spread from 0.1 to 3 THz. The structure of the spectrum (position of the local maxima) depends on the thickness of the layer, parameters of the substrate (BK7 or air gap), and duration and energy of the pump pulse. Numerous narrow dips in the spectra are identified as absorption lines of water vapor. For a type I sandwich structure with a = 50 μm, the position of the main maximum of the spectrum is localized near 0.8−1.2 THz (see Fig. 2(a)), and for a = 30 μm, the spectrum maximum is shifted to the higher frequency ~1.5 THz in accordance with the theoretical prediction in [28].

Modulation of the spectrum resulted from the interference of two quasi-plane waves of the Čerenkov wedge: the first wave is emitted directly to the Si prism through the upper facet of the LN layer (upper wave) and the second wave is partially reflected from the lower facet (lower wave). For a type II scheme, due to the total reflection of the lower wave, this interference is more pronounced and results in appearance of two peaks near 0.8 *THz* and 2.5 *THz* (independent of the air gap). By moving the metal plate from ∞ to the LN layer, the spectrum is changed as follows. The low-frequency spectral components increase near 0.8 *THz* and decrease near 2.5 *THz*, and a dip in the spectrum near 1.5 *THz* shifts to a higher frequency. This effect is explained by different phase shifts of the lower wave reflected from the lower LN facet for different air gaps [29]. Note that this spectral turning occurred for $0 < b < 20 \ \mu m$ where the evanescent terahertz field is localized. By varying the energy of the optical pump, we observed an increase in the high-frequency spectral component (see Fig. 2(a)), which can be attributed to the pump self-focusing. Indeed, such an instability causes a decrease in the transverse size of the optical pulse. According to [28], this should enhance the generation of the higher-frequency components in the terahertz spectrum. Increasing pulse duration also modifies the spectrum, but its modification depends on the chirp sign (see inset in Fig. 2). For the positive chirp, the high-frequency components are suppressed with increasing pulse duration, which can easily be explained by the
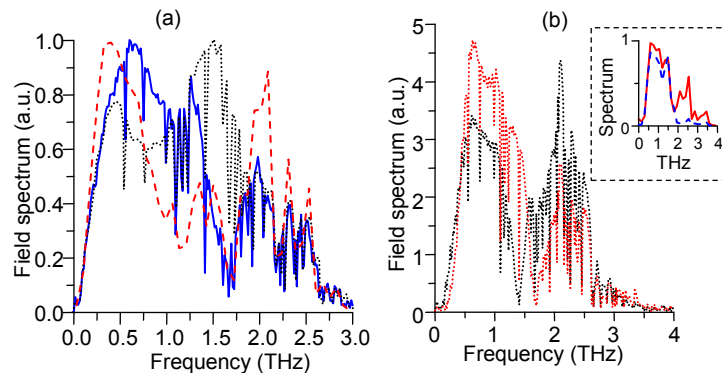

Fig. 2 Terahertz spectra generated in (a) type I sandwich structures with $a = 50 \ \mu m$ (solid curve) and 30 μm (dotted curve) by a 50-*fs* laser pulse with the energies $W = 17 \ \mu J$ and 10 μJ, respectively, dashed curve shows the spectra for $a = 50 \ \mu m$, $\tau = 200 \, fs$, and $W = 130 \ \mu J$; (b) type II sandwich structures with $b = 0$ (solid curve) and $b > 20 \ \mu m$ (dotted curve) by a 50-*fs* laser pulse with 5-μJ energy. Terahertz field spectra for a 16-μJ laser pulse with positive (dashed) and negative (solid) chirp and 150-*fs* duration ($b = 0$) are given in the inset. This figure was taken from [22, 23].

increasing duration of nonlinear polarization as a source of THz radiation. For the negative chirp, this effect was observed for long pulses (>200 *fs*), while for the shorter pulse duration ($50 < \tau < 200 \, fs$) the spectrum did not significantly change. Indeed, due to the material dispersion, the laser pulse spreads from 50 to 200 *fs* in a 1-*cm* long LN crystal; thus, an average pulse duration of the optical pulse with negative dispersion in the interval $50 < \tau < 200 \, fs$ varies little and the THz spectrum should not significantly change.

Figure 3(a) shows the efficiency of the optical-to-terahertz conversion as a function of the pump energy for different chirped pulse durations. For a type II structure, we obtained an almost twofold increase in the THz energy due to the one-direction concentration of THz radiation: in a type I structure, one-half of the THz radiation is absorbed in the BK7 substrate, while in a type II structure almost all generated radiation was output from the Si prism (due to the total reflection of the lower Čerenkov wedge). The conversion efficiency grows linearly with the optical energy and then saturates. The saturation level weakly depends on the chirp for a pulse duration of less than 200 *fs* and decreases for the longer pulses. Note that we have not observed a decrease in the pump transmission through the LN layer with increasing pump energy. Thus, the saturation of the THz conversion efficiency results mainly from the pulse distortion due to self-focusing rather than from three-photon absorption of the pump pulse. Maximum conversion efficiency (for a type II structure) as high as 0.25% is achieved for a pulse duration of 50–150 *fs* and an optical pump energy of 15–20 *μJ* (with a fluence of ~ 25 *mJ/cm²*). Maximum slope of the dependence in Fig. 3(a) is obtained for the laser pulse with negative chirp and a duration of 100–150 *fs*. Over the whole optical energy range, the efficiency for the negative chirp dominates the efficiency for the positive chirp (cf. the empty and filled circles in Fig. 3(a)). The influence of the chirped pulse duration on the conversion efficiency is shown in more detail in Figs. 3(b) and 3(c). For a low pump energy (see Fig. 3(b)) in the case of the positive chirp, the efficiency decreases monotonically with the pulse duration, while for the negative chirp, the efficiency rises by 30%–40% near the 100-*fs* pulse duration and then decreases monotonically. In the pulse duration interval 100–400 *fs*, the efficiency is approximately two times higher for the negative chirp
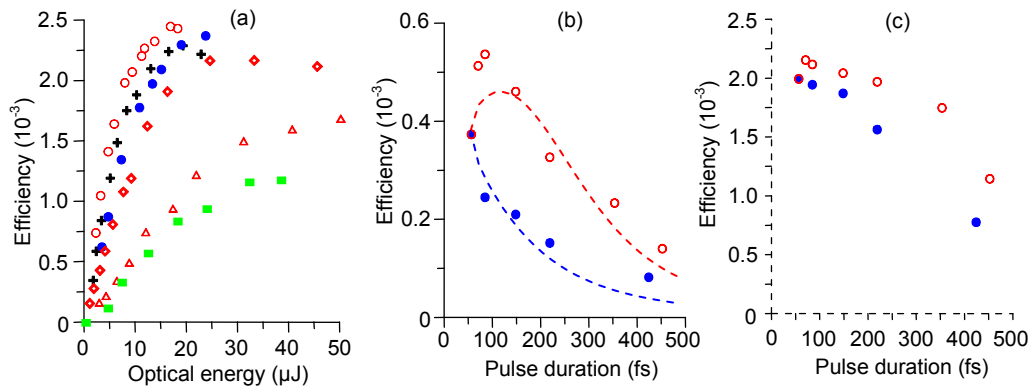

Fig. 3 (a) Conversion efficiency as a function of the laser pulse energy for a type II sandwich structure at *b* = 0 for a pulse duration of 50 *fs* (crosses), 150 *fs* with positive and negative chirp (filled and empty circles, respectively), 220 *fs* (diamonds), and 400 *fs* (triangles) with negative chirp. Filled boxes depict efficiency for a type I sandwich structure with *a* = 50 *μm* and τ = 50 *fs*. Conversion efficiency as a function of the laser pulse duration with positive (filled circles) and negative (empty circles) chirp for (b) 2-*μJ* and (c) 18-*μJ* pump energies. Dashed curves correspond to the theoretical calculation (taken from [22, 23]).

compared to the positive chirp with the same pulse duration. Theoretical calculation (dotted lines in Fig. 3(b)) based on the theory developed in [29] with allowance for pulse distortion agrees well with the experiment. For a high pump energy (Fig. 3(c)), the efficiency is almost independent of

the chirp sign and pulse duration for up to 150 *fs*. For the longer pulse durations, the efficiency decreases monotonically independent of the chirp sign.

3. Terahertz generation by tilted-front laser pulses in a LiNbO₃ crystal

The tilted pulse front technique has been studied both experimentally and theoretically by many authors. Theoretical calculations predict an optical-to-terahertz conversion efficiency as high as a few percent at room temperature and even several times higher for a cryogenically cooled LN crystal [30-32], but experimental studies have shown that the efficiency saturates near 0.1-0.2 % [10-15, 33]. The origin of the observed saturation is not well understood and is under discussion [15, 30]. Below we will show that saturation is caused by self-phase modulation of the optical pump and the advantage of a relatively long pulse duration for THz generation predicted by theory [30, 31] is true only before the efficiency saturation.

A schematic of the experiment for THz generation in the LiNbO₃ crystal by tilted laser pulses is shown in Fig. 4. A Ti:Sa laser system ($\lambda = 795$ *nm*, 10 *Hz*, 10 *mJ*, 70 *fs*) was used as the optical pump. Tilted laser pulse was produced by a diffraction grating (2000 *mm*$^{-1}$) and imaged by a spherical mirror (F = 306 *mm* and D = 50 *mm*) in the LN crystal (stoichiometric 1 *mol.* % MgO-doped LiNbO₃) with required intensity front tilt angle $\alpha \sim 63°$. The crystal had a 7.6 *mm* × 7.6 *mm* entrance face, was 15 *mm* long, and was placed in a He-cooled cryostat with temperature control ranging from $T = 4$ *K* to 293 *K*. While propagating in the LN crystal (along the *z* axis), the tilted optical pulse generates THz radiation perpendicular to the pump intensity front. To lead the THz pulses through an output window of the cryostat, a quartz prism with a tip angle of 21° was placed at the exit face of the LN crystal. The experimental scheme was aligned [30] at each crystal temperature to maximize the THz generation efficiency. To measure the energy of THz radiation, a calibrated Golay cell (Tydex) was placed ~ 1 *cm* from the output window of the cryostat. A spatiotemporal THz field structure was explored using the EO sampling technique.
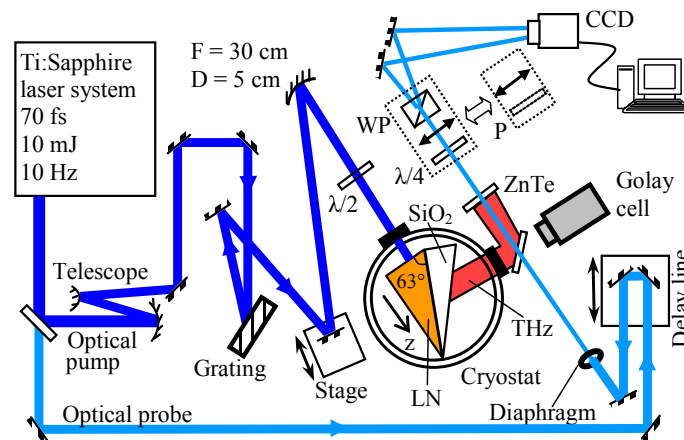

Fig. 4 Experimental setup for THz generation in the LiNbO₃ crystal by laser pulses with tilted intensity front.

The optical-to-terahertz energy conversion efficiency η as a function of the pump energy W (and fluence F) is shown in Fig. 5 for different pulse durations τ, crystal lengths L, and temperatures T. Several conclusions can be drawn from this figure. First, there are two regimes of THz generation depending on the pump energy. In the weakly nonlinear generation regime corresponding to a low pump energy, η depends linearly on W. In the strongly nonlinear generation regime, where W is higher than some threshold value W_{th} (corresponding to the fluence F_{th}), the efficiency saturates and even decreases. Second, the threshold fluence depends on pulse duration and crystal length, but does not depend on temperature. Third, in different generation regimes the maximum efficiency was attained with different parameters $[L,\tau]$. In the weakly nonlinear generation regime, η is maximized at long $L = 10$ mm and $\tau = 200$ fs and is minimized at short $L = 5$ mm and $\tau = 120\,fs$, while in the strongly nonlinear generation regime the optimal parameters are inverted: the maximum η is achieved for [5 mm, 120 fs (200 fs)] and the minimum η, for [10 mm, 200 fs]. Fourth, the efficiency increases when the temperature drops down and reaches its highest value of ~ 0.2 % at $T = 77$ K for $L = 5$ mm at $\tau = 120\,fs$ and $200\,fs$.
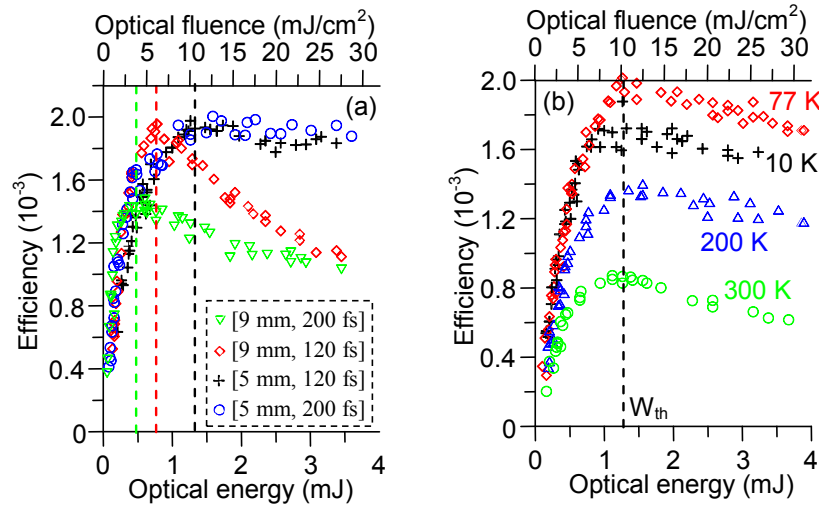

Fig. 5 Efficiency as a function of the pump energy (fluence) for (a) T = 77 K with different [L,τ]: crosses -- [5 mm, 120 fs], circles -- [5 mm, 200 fs], diamonds -- [9 mm, 120 fs], triangles -- [9 mm, 200 fs]; (b) fixed [5 mm, 120 fs] and different temperatures. This figure was taken from [24].

Increasing efficiency with decreasing temperature can be explained by the decreasing THz absorption [34]. Higher efficiency for large L and long τ in the weakly nonlinear generation regime agrees well with the theories developed earlier [30-32]. The increase in η with increasing L is interpreted as an increase in the interaction length between the THz radiation and the optical pump [32]. The dependence of η on τ is non-monotonic [30, 31]: the increase in τ results, on the one hand, in decreasing incident pump intensity which decreases the THz energy and, on the other hand, in increasing dispersion length which increases the THz energy. In the case considered, dispersion wins this competition, and the maximum efficiency is obtained for a longer (200 fs) pulse duration.

Large L and long τ in the strongly nonlinear generation regime (high W) did not yield the maximum efficiency because of the low value of F_{th} under efficiency saturation. We suppose that the saturation is a result of deformation of the laser intensity front (or detuning from the optimal tilt angle) due to nonlinear self-phase modulation (SPM) of the optical pump. Indeed, the nonlinear phase acquired by the laser pulse in the LN crystal with allowance for the angular dispersion can be estimated as of the order of unity under efficiency saturation for different τ, L, and T [24]. The assumption of efficiency saturation as due to terahertz free-carrier absorption (FCA) [30, 31, 12] contradicts some facts. First, as was mentioned in Sec. 2, we did not observe the optical pump attenuation in a 1 *cm*-long LN layer within a few percent even for a tenfold higher intensity (200-300 GW/cm^2) compared with the present work. With account of this observation, estimated maximum photo-excited electron density in the present experiment is about $3 \cdot 10^{13}$ cm^{-3} and cannot lead to a significant absorption of THz radiation. Second, it was demonstrated that photo-excited free carriers in the LN crystal are trapped as small polarons within 100-200 *fs* [35, 36]. Such polarons have a binding energy of ~1 *eV* and actually do not interact with THz radiation. Thus, the lifetime of free carriers in LN is much less than the THz pulse duration, which significantly suppresses the FCA. Third, if nevertheless the FCA is strong enough to affect the efficiency saturation, some variation in F_{th} may be expected when the crystal is cooled due to the temperature dependence of the scattering coefficient [37] (and recombination rate [38]), which changes the THz absorption [39-41]. But we did not observe the dependence of F_{th} on temperature (see Fig. 5(b)). In addition, it is seen in Fig. 6(a) that in the weakly nonlinear generation regime there was a spectrum broadening of up to 2 *THz* with the maximum near 0.5 *THz*, while in the strongly nonlinear generation regime, the spectrum narrowed to 1.5 *THz* with a slightly red-shifted maximum. This observation may result from the pump SPM and can be explained by the detuning from the optimal tilt angle which, according to [42], leads to a decrease in the high terahertz frequency components. At the same time, the FCA model should lead to a stronger absorption of the low-frequency spectral components with increasing pump energy (according to the Drude model), in contradiction to the experiment.
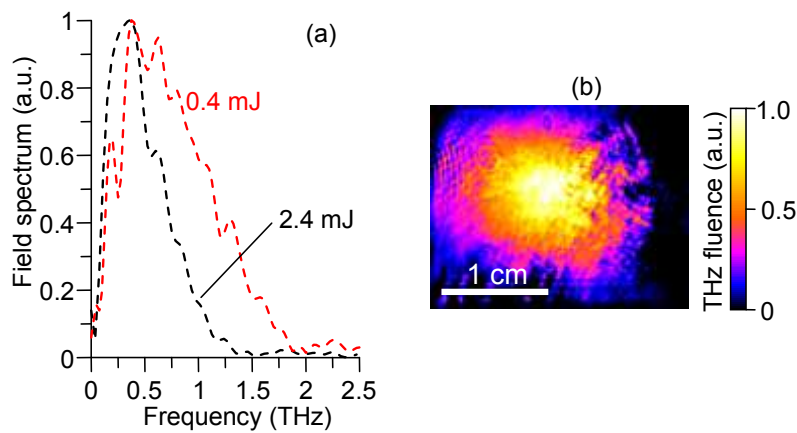

Fig. 6 (a) Terahertz field normalized spectra for different pump energies; (b) 2D THz beam profile at a distance of 67 *cm* from the LN crystal. T = 293 *K*, τ = 200 *fs*, and L = 5 *mm*. This figure was taken from [24].

The transverse distribution of terahertz fluence in the strongly nonlinear generation regime (measured by depolarization of the probe optical beam in the ZnTe crystal) is shown in Fig. 6(b). The distribution is smooth and has a nearly symmetric Gaussian form with horizontal and vertical FWHM transverse sizes of 10 *mm* and 9 *mm*, respectively. The vertical size agrees well with the THz beam diffraction estimated by the size of the THz source (determined by the optical beam), whereas the horizontal size exceeds the diffraction limit, which can be explained by the bending of the tilted intensity front due to optical imaging [30] and the horizontal THz beam deformation due to pump SPM. The latter assumption is corroborated by the fact that the pump energy variation in the 2-3 *mJ* range was accompanied by changes in the horizontal THz beam distribution (not shown), whereas the vertical distribution was preserved.

4. Two-color laser-plasma generation of terahertz radiation using a frequency-tunable half harmonic of the femtosecond pulse

In this part of the paper we discuss our results of experimental and theoretical studies of low-frequency terahertz emission from the ambient air ionized by a two-color femtosecond laser pulse containing the fundamental-frequency main field and a weak additional field tunable near the half-harmonic frequency. The situation considered here is in contrast to almost all the previous publications on two-color THz generation in gases where as the additional field the second harmonic of the fundamental frequency was used. The additional field that is tunable near the half-harmonic frequency was produced by the optical parametric amplifier (OPA). It can be said that this scheme is inverted with respect to the common two-color scheme since the double-frequency field is the main strong field in this case. The use of lower-frequency pump fields produced by OPA can increase the efficiency of THz generation, as shown in [43], where the OPA-generated frequency-tunable pulse and its second harmonic were utilized. Moreover, the dephasing length determined by the air dispersion [44, 45] for two-color pulses with waves at 800 and 1600 *nm* is fourfold greater than that for the pulses with waves at 800 and 400 *nm* (10 *cm* against 2.5 *cm*). This permits using a looser focusing of the laser pulse and a longer plasma filament without the destructive interference of THz radiation [46], thus potentially achieving a higher THz yield.

The experimental setup and the theoretical model were described in detail previously [25]. Here, we just point out the most interesting peculiarities of our results. In the experiments, we observed several effects which are important both for the THz yield control and for the development of a theoretical model (see Fig. 7). First, this concerns the dependences of the horizontal and vertical components of the THz yield on the angle θ between the fundamental frequency field (oriented horizontally) and the half-harmonic field (Fig. 7(a)). For a smaller θ, the THz polarization is mainly horizontal and the THz yield is maximal. The horizontal component of the THz field decays while the vertical one rises and reaches a maximum at $\theta \approx \pi/4$ as θ

increases. For a greater θ, both components fall, reaching almost a zero value at $\theta = \pi/2$. Second, the THz yield with independent variations in average powers of the fundamental and half-harmonic fields was measured. We observed quadratic dependence of the THz yield on the half-harmonic power, while the dependence on the fundamental-harmonic power demonstrates a very strong rise with some threshold (Fig. 7(b)). Finally, we observed that when the half-harmonic frequency is changed, the dependence of the THz yield on the half-harmonic detuning frequency is of a resonant-like shape, with the maximum near the zero detuning and a half-width of about 5 *THz* (Fig. 7(c)). At the same time, the low-frequency THz spectrum recovered from the autocorrelation measurements (Fig. 7(d)) does not depend on the detuning and has both the center frequency f_{THz} and a width of about 1.5 *THz* at the half-peak level (see Fig. 7(e)).
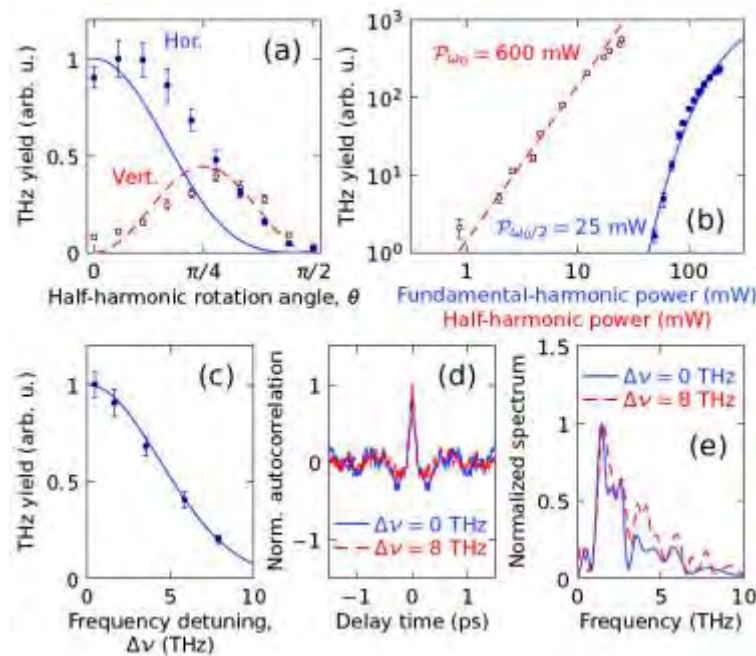

Fig. 7 (a)–(c) The THz yield as a function of the parameters of a two-color femtosecond pulse containing fundamental and half-harmonic fields (the points are the experimental results, and the lines are obtained using analytical formulas; error bars correspond to the maximum and minimum values in a series of measurements). (a) Dependences of the horizontal (filled dots and solid line) and vertical (hollow dots and dashed line) polarization of the THz radiation on the angle between the fundamental and half-harmonic fields θ for average powers of the fundamental harmonic $P_{\omega 0} = 600$ *mW* and the half-harmonic $P_{\omega 0/2} = 30$ *mW*. (b) Dependence of the THz yield on $P_{\omega 0/2}$ for fixed $P_{\omega 0} = 600$ *mW* (hollow dots and dashed line) and dependence of the THz yield on $P_{\omega 0}$ for fixed $P_{\omega 0/2} = 25$ *mW* (filled dots and solid line). (c) Dependence of the THz yield on the additional-field frequency detuning (with respect to the half-harmonic frequency) for $P_{\omega 0} = 500$ *mW* and $P_{\omega 0/2} = 25$ *mW*. (d). (e) Normalized autocorrelation functions (d) measured experimentally with (dashed line) and without (solid line) the frequency detuning and the corresponding normalized THz spectra (e) for $P_{\omega 0} = 500$ *mW* and $P_{\omega 0/2} = 25$ *mW*. This figure was taken from [25].

To explain the results of the experiment, we use an approach based on the residual current density (RCD) model [25]. According to this model, the residual current $\mathbf{j}_{RCD}$ causing the THz generation is given by the expression

$$\mathbf{j}_{RCD} \approx j_{osc}\left(\alpha\beta^{1/2}\Omega_a\tau_i/2\right)\cdot\left(E_a/E_1\right)^{3/2}e^{-\beta E_a/E_1}e^{-2(\tau_i\Delta\omega)^2}\left(E_{1/2}/E_1\right)^2\mathbf{\Phi}(\phi,\theta),\tag{1}$$

$$\mathbf{\Phi}(\phi,\theta)=-\sin(2\phi)\left[3\cos^2\theta\cdot\hat{\mathbf{x}}+2\sin(2\theta)\hat{\mathbf{y}}\right],\tag{2}$$

$$\tau_i=\tau_p\sqrt{E_1/4\ln 2\beta E_a}\,,\tag{3}$$

where E_1 and $E_{1/2}$ are the fundamental and half-harmonic amplitudes; $j_{osc}=e^2N_gE_1/m\omega_0$ is the oscillatory current density in the fundamental field, τ_p is the pulse duration (at FWHM), $\Delta\omega$ is the small detuning of the half-harmonic frequency, ϕ is the phase shift between the additional and fundamental fields, N_g is the gas density, $E_a = 5.14 \times 10^9$ *V/cm* and $\Omega_a = 4.13 \times 10^{16}$ s^{-1} are the atomic units of the field and frequency; $\alpha = 4(I_{N2}/I_H)^{5/2}$ and $\beta = (2/3)(I_{N2}/I_H)^{3/2}$; $I_{N2} = 15.6$ *eV* and $I_H = 13.6$ *eV* are the ionization potentials of a nitrogen molecule and a hydrogen atom.

Analytical formula (1) represents RCD as the product of separate functions. This allows one to compare easily the theory and the experimental results. First, this concerns the dependences of the horizontal and vertical components of the THz yield $P_{hor}\propto j_{RCD}^2\propto 9\cos^4\theta$ and $P_{vert}\propto j_{RCD}^2\propto 4\sin^2 2\theta$ on the angle θ (see solid and dashed lines in Fig. 7(a)). Second, the formula perfectly describes the dependence of the THz yield on the half-harmonic power for a fixed fundamental-harmonic power (dashed line in Fig. 7(b)). Formulas (1) and (2) are in good agreement with the experimentally measured dependences of the THz yield on the power at the fundamental frequency (solid line in Fig. 7(b)) and the frequency detuning $\Delta\nu=\Delta\omega/2\pi$ (see Fig. 7(c)). Note that the dependence on $\Delta\nu$ is a resonant-like curve with $\sqrt{\ln 2}/2\pi\tau_i$ at FWHM.

5. Plasma filament study by transverse terahertz scattering

Filamentation of the intense femtosecond laser pulses propagating in atmospheric air was first observed in the experiments about 15 years ago and has become a field of intense research activity [47]. The role of the laser-induced plasma which stops self-focusing of the laser beam is very important in the filamentation. Dynamic balance between the self-focusing and the plasma defocusing results in creation of a long plasma channel and laser pulse propagation with suppressed diffraction, which is attractive for possible practical applications such as remote sensing or lightning control.

Although the plasma density and the rate of plasma decay are crucial parameters for many applications, their correct measurement is not straightforward. To measure plasma densities over a large range of electron densities, we propose the technique of transverse terahertz scattering of

pulsed THz radiation from the filament [26]. In our experiment, we demonstrated applicability of this technique for plasma density decay measurements in the range 10^{17}- 10^{15} cm^{-3}.
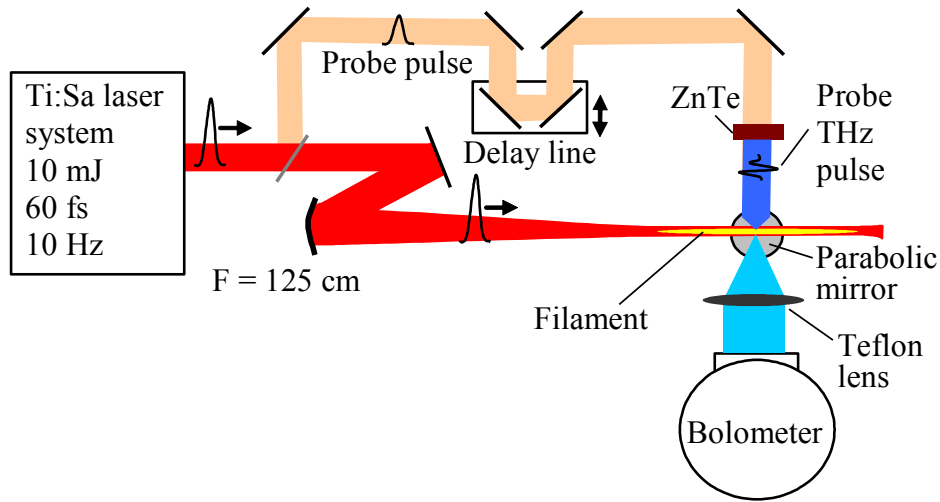

Fig. 8 Experimental setup for terahertz scattering measurements.

The experimental setup is presented in Fig.8. A Ti:Sa laser system generating 60-*fs* FWHM laser pulses at the 795-*nm* central wavelength with 10-*Hz* repetition rate was used to create and probe a plasma filament. The system provided an energy of up to 10 *mJ* in the laser pulse. The radius of the beam was 5 *mm* (at $1/e^2$). The laser pulse was focused in ambient air under atmospheric pressure by a spherical mirror of 125-*cm* focal length. The plasma filament was formed near the focal plane. The observed length of the plasma channel was 1-10 *cm*, depending on the laser pulse energy. Part of the laser pulse was split from the main (pump) pulse before the focusing and was used as a probe pulse. For transverse terahertz scattering measurements, the probe pulse (after the delay line) generated a pulse of THz radiation in a 1-*mm* thick ZnTe crystal. The pulse duration was ~1 *ps* with the maximum of the spectrum near 1 *THz*. The THz pulse was focused on the plasma filament by an off-axis parabola with the focal length $F = 5$ *cm*. The terahertz radiation scattered from the plasma in the perpendicular direction (90° scattering angle) was collected by a teflon lens ($F = 4$ *cm*, $D = 4$ *cm*) into a liquid He-cooled InSb hot electron bolometer (QMS Instruments, QFI/4 model).

For terahertz radiation (0.3-3 *THz*), a critical plasma density lies in the range 10^{15}-$10^{17}cm^{-3}$. Thus, scattering of THz radiation from the plasma filament with transverse diameter comparable to the THz wavelength is very sensitive to the electron density in this range. Following this idea, we explored the plasma decay by measuring the scattering of the probe THz pulse as a function of time delay using the bolometer (Fig. 9(a)).
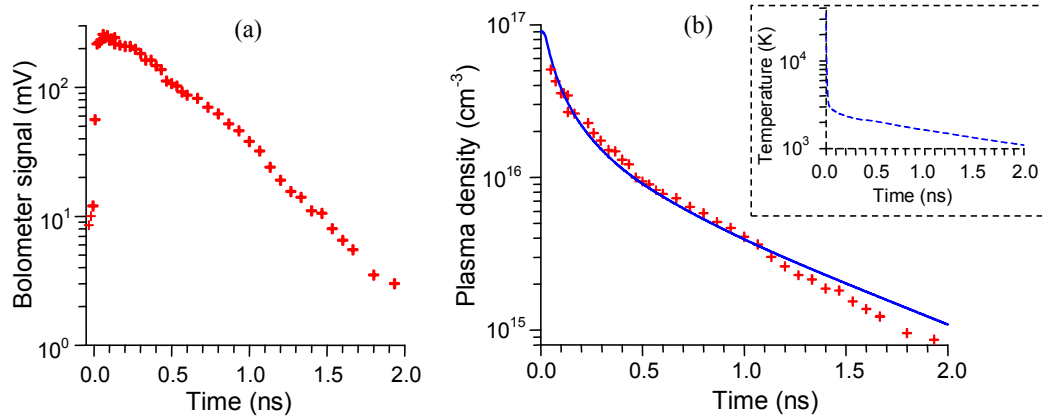
Fig. 9 (a) Bolometer signal as a function of time delay. (b) Plasma density N_{e0} decay. Crosses correspond to the terahertz experimental measurement and the solid curve, to the theoretical calculation. The inset shows the electron temperature as a function of time. This figure was taken from [26].

To obtain the plasma density N_{e0} from the scattered THz signal, a numerical code calculating radiation scattering by an axial symmetric cylinder with an arbitrary transverse distribution of the electron density was developed. The result of plasma density calculation obtained from THz scattering data is shown in Fig. 9(b) by crosses. It follows from Fig. 9(b) that the plasma density in a filament demonstrates a fast decrease by two orders of magnitude (from $\sim 10^{17}$ *cm*$^{-3}$ to 10^{15} *cm*$^{-3}$) on a 2-*ns* time scale.

Detailed analysis has shown that among the numerous plasma chemical reactions which may occur in atmospheric air [48], only several processes make a significant contribution to the plasma density decay after the filament formation (over a time period of 2 *ns*). The reactions included in our calculation are as follows. Five channels of electron recombination were taken into account, namely, dissociative and three-body electron recombinations with O_2^+ and dissociative electron recombination with complex ions $N_2O_2^+$, O_4^+, and $H_2O \cdot O_2^+$ formed in atmospheric air during the decay. We used a 50% relative humidity in our calculations. Note that the electron attachment to O_2 molecules plays a minor role on our time scale and was not considered in the calculation.

The considered rate coefficients strongly depend on electron temperature T_e. The temporal evolution of T_e was calculated from a numerical solution of the electron energy conservation equation [49]. The frequency of electron energy relaxation in collisions with molecules was obtained using a computer code [50]. This code solves the Boltzmann equation for electrons taking into account the electron energy losses due to electronic, vibrational, and rotational excitation of N_2 and O_2 and elastic scattering of electrons by charged particles and molecules. Due to a high electron-electron collision frequency because of the high ionization degree, the electron energy distribution function was assumed to be Maxwellian in our experiment. The gas temperature was assumed to be 293 *K*. Calculated electron temperature is shown in the inset in Fig. 9(b). According to our analysis, a rapid (within several tens of ps) temperature decrease to

~3000 K results from the electronic and vibrational excitation of molecules followed by a temperature decrease due to rotational excitation.

The time evolution of the electron density (solid curve in Fig. 9(b)) was calculated on the basis of the above-mentioned and calculated electron temperatures. Good agreement is observed between the experimental results and the calculations. It follows from our calculations that in the first nanosecond the reactions of dissociative and three-body recombinations with O_2^+ ion play the main role in the plasma density decrease. On a larger time scale, the recombination with complex ions dominates. Yet, all the five channels of electron losses are important for provision of a qualitative agreement with the experimental data.

The rapid plasma decay observed in the experiments imposes significant limits on filament applications such as lightning protection, atmospheric remote sensing, and so on. To increase the plasma lifetime, several approaches were proposed [51-55]. One of the ideas is application of an external electric field [55] that we studied both experimentally and theoretically in [27]. To do this, two circular plane electrodes (25 cm in diameter) with pinholes (2 mm in diameter) in the center for transmission of laser radiation were placed coaxially with the filament at a distance of 5 cm, so as the filament fully overlapped the gap between the electrodes. High voltage was applied between the electrodes to induce external electric field E in the region of the plasma filament. Due to the air discharge stimulated by the filament, the maximum electric field was limited to 7–8 kV/cm.
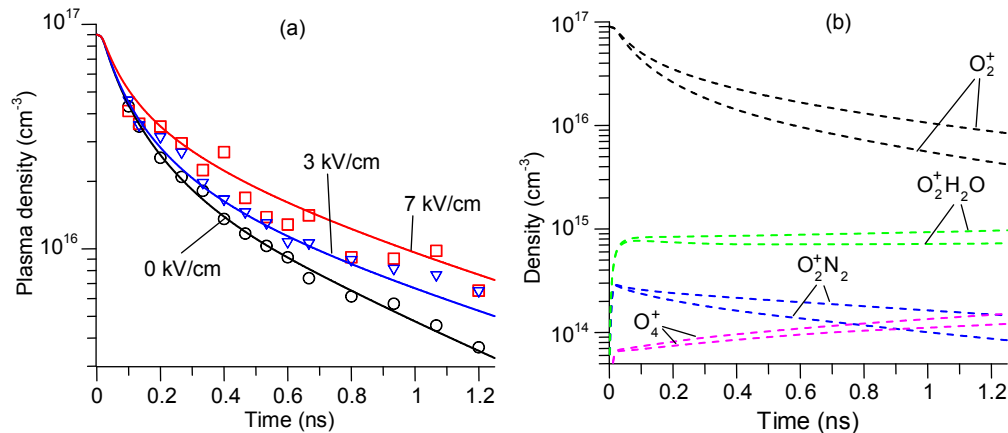

Fig. 10 (a) Time evolution of electron density during plasma decay for different values of the external electric field E. The symbols correspond to our measurements and the curves, to the calculations. (b) Time evolution of ion densities during plasma decay at $E = 0$ (dashed curves) and at $E = 7$ kV/cm (solid curves). This figure was taken from [27].

For a study of plasma density decay in the external electric field, we measured the scattering of the probe terahertz pulses in the same manner as discussed above. The results of our measurements for several values of the electric field are presented in Fig. 10(a). The main conclusion that can be made from the presented data is that the rate of the plasma decay decreases

in the presence of an external electric field, but rather moderately. For example, the plasma density for a 1-*ns* time delay and $E = 7$ *kV/cm* is approximately twice as large as that for $E = 0$.

Our theoretical research is based on the approach developed in [26], which was extended by taking into account the external electric field. We considered electron heating in an external electric field that affects the rates of electron-ion recombination. The set of reactions governed by the plasma decay was the same as that we discussed when the decay in the absence of the electric field was considered. The results of theoretical calculations are shown in Fig. 10(a) by dashed and solid lines. It appears that information on the rate of three-body recombination with the participation of molecular ions is scanty, and the rate of this process is known to the least accuracy among the reaction rates. To reach agreement between the calculation and the experiment, we increased by 5-10 *times* (depending on the electron temperature) the rate of three-body recombination of molecular ions compared with the value for H+ ions calculated in [56] for the same range of electron densities. Figure 10(b) illustrates the dynamics of ion densities during the plasma decay in an external electric field.

5. Conclusions

Efficient THz generation with an optical-to-terahertz conversion efficiency of 0.1-0.25% was demonstrated when intense femtosecond laser radiation propagated in a $LiNbO_3$ crystal for two geometries of the experiment, namely, a sandwich structure and a tilted intensity front geometry. We also examined the conversion efficiency saturation mechanism which we attribute to the femtosecond pulse distortion due to the Kerr nonlinearity. Terahertz emission from the ambient air ionized by a two-color femtosecond laser pulse containing the fundamental-frequency main field and a weak additional field tunable near the half-harmonic frequency was studied both experimentally and theoretically. The model based on the free-electron residual current density assumption give a good agreement with the experimental results. We developed a THz scattering technique for measurement of the air plasma density decay in a filament produced by an intense femtosecond laser pulse and demonstrated a two order of magnitude (from 10^{17} *cm*$^{-3}$ to 10^{15} *cm*$^{-3}$) decay of the electron density within 2 *ns*. It was shown that the application of an additional external electric field decreases the plasma decay rate.

References

1. M. Beck, H. Schäfer, G. Klatt, et. al.. "Impulsive terahertz radiation with high electric fields from an amplifier-driven large-area photoconductive antenna". *Opt. Express*, 18, 9251-9257 (2010).

2. T. Löffler, T. Hahn, M. Thomson, et. al.. "Large-area electro-optic ZnTe terahertz emitters". *Opt. Express*, 13, 5353-5362 (2005).

3. S. Vidal, J. Degert, M. Tondusson, et. al.. "Impact of dispersion, free carriers, and two-photon absorption on the generation of intense terahertz pulses in ZnTe crystals". *Appl. Phys. Lett*., 98, 191103 (2011).

4. F. Blanchard, L. Razzari, H.-C. Bandulet, et. al.. "Generation of 1.5 μJ single-cycle terahertz pulses by optical rectification from a large aperture ZnTe crystal". *Optics Express*, 15, 13212-13220 (2007).

5. J. Hebling, A.G. Stepanov, G. Almási, et. al.. "Tunable THz pulse generation by optical rectification of ultrasort laser pulses with tilted pulse fronts". *Appl. Phys. B*, 78, 593-599 (2004).

6. Y.-S. Lee, T. Meade, V. Perlin, et. al.. "Generation of narrow-band terahertz radiation via optical rectification of femtosecond pulses in periodically poled lithium niobate". *Appl. Phys. Lett.*, 76, 2505 (2000).

7. J.A. L'huillier, G. Torosyan, M. Theuer, et. al.. "Generation of THz radiation using bulk, periodically and aperiodically poled lithium niobate – Part 2: Experiments". *Appl. Phys. B*, 86, 197–208 (2007).

8. J. Hebling, G. Almási, I. Z. Kozma, et. al.. "Velocity matching by pulse front tilting for large-area THz pulse generation". *Opt. Express*, 10, 1161-1166 (2002).

9. G. Xu, X. Mu, Y. J. Ding, et. al.. "Efficient generation of backward terahertz pulses from multiperiod periodically poled lithium niobate". *Opt. Lett.*, 34, 995-997 (2009).

10. A.G. Stepanov, L. Bonacina, S.V. Chekalin, et. al.. "Generation of 30 μJ single-cycle terahertz pulses at 100 *Hz* repetition rate by optical rectification". *Opt. Lett.*, 33, 2497- 2499 (2008).

11. A.G. Stepanov, S. Henin, Y. Petit, et. al.. "Mobile source of high-energy single-cycle terahertz pulses". *Appl. Phys. B*, 101, 11-14 (2010).

12. J.A. Fülöp, L. Pálfalvi, S. Klingebiel, et. al.. "Generation of sub-mJ terahertz pulses by optical rectification". *Opt. Lett.*, 37, 557-559 (2012).

13. H. Hirori, A. Doi, F. Blanchard, et. al.. "Single-cycle terahertz pulses with amplitudes exceeding 1 *MV/cm* generated by optical rectification in LiNbO$_3$". *Appl. Phys. Lett.*, 98, 091106 (2011).

14. A. G. Stepanov, J. Hebling, and J. Kuhl. "THz generation via optical rectification with ultrashort laser pulse focused to a line". Appl. Phys. B 81, 23-26 (2005).

15. A.G. Stepanov, J. Kuhl, I.~Z. Kozma, et. al.. "Scaling up the energy of THz pulses created by optical rectification". *Opt. Express*, 13, 5762-5768 (2005).

16. M. Theuer, G. Torosyan, C. Rau, et. al.. "Efficient generation of Cherenkov-type terahertz radiation from a lithium niobate crystal with a silicon prism output coupler". *Appl. Phys. Lett.,* 88, 071122 (2006).

17. D. J. Cook and R. M. Hochstrasser. "Intense terahertz pulses by four-wave rectification in air". *Opt. Lett.*, 25, 1210-1212 (2000).

18. M.D. Thomson, M. Kreß, T. Löffler, et. al.. "Broadband THz emission from gas plasmas induced by femtosecond optical pulses: From fundamentals to applications". *Laser & Photon. Rev.*, 1, 349–368 (2007).

19. B. Clougha, J. Daia, and X.-C. Zhang. "Laser air photonics: beyond the terahertz gap". *Materials Today*, 15, 50-58 (2012).

20. M.D. Thomson, V. Blank, and H.G. Roskos. Terahertz white-light pulses from an air plasma photo-induced by incommensurate two-color optical fields. *Opt. Express*, 18, 23173-23182 (2010).

21. Y. Minami, T. Kurihara, K. Yamaguchi, et. al.. "High-power THz wave generation in plasma induced by polarization adjusted two-color laser pulses". *Appl. Phys. Lett.*, 102, 041105 (2013).

22. S.B. Bodrov, M.I. Bakunov, B.V. Shishkin, et. al.. "Highly efficient optical-to-terahertz conversion in a sandwich structure with LiNbO3 core". *Opt. Express*, 17, 1871-1879 (2009).

23. S.B. Bodrov, I.E. Ilyakov, B.V. Shishkin, et. al.. "Efficient terahertz generation by optical rectification in Si-LiNbO3-air-metal sandwich structure with variable air gap". *Appl. Phys. Lett.*, 100, 201114 (2012).

24. S. B. Bodrov, A. A. Murzanev, Yu. A. Sergeev, et. al.. "Terahertz generation by tilted front technique in weakly and strongly nonlinear regimes". *Appl. Phys. Lett.* 103, 251103 (2013).

25. N.V. Vvedenskii, A.I. Korytin, V.A. Kostin, et. al.. "Two-color laser-plasma generation of terahertz radiation using a frequency-tunable half harmonic of a femtosecond pulse". *Phys. Rev. Lett.*, accepted.

26. S. Bodrov, V. Bukin, M. Tsarev, et. al.. "Plasma filament investigation by transverse optical interferometry and terahertz scattering". *Opt. Express*, 19, 6829-6935 (2011).

27. S. Bodrov, N. Aleksandrov, M. Tsarev, et. al.. "Effect of an electric field on air filament decay at the trail of an intense femtosecond laser pulse". *Phys. Rev. E*, 87, 053101 (2013).

28. S.B. Bodrov, M.I. Bakunov, and M. Hangyo. "Efficient Čerenkov emission of broadband terahertz radiation from an ultrashort laser pulse in a sandwich structure with nonlinear core". *J. Appl. Phys.,* 104, 093105 (2008).

29. M.I. Bakunov, S.B. Bodrov. "Si–LiNbO3–air–metal structure for concentrated terahertz emission from ultrashort laser pulses". *Applied Physics B.*, 98, 1-4 (2010).

30. J.A. Fülöp, L. Pálfalvi, G. Almási, et. al.. "Design of high-energy terahertz sources based on optical rectification". *Opt. Express*, 18, 12311 (2010).

31. J.A. Fülöp, L. Pálfalvi, M.C. Hoffmann, et. al.. "Towards generation of mJ-level ultrashort THz pulses by optical rectification". *Opt. Express,* 19, 15090-15097 (2011).

32. M.I. Bakunov, S.B. Bodrov, and E.A. Mashkovich. "Terahertz generation with tilted-front laser pulses: dynamic theory for low-absorbing crystals". *J. Opt. Soc. Am. B*, 28, 1724-1734 (2011).

33. M.C. Hoffmann, K.-L. Yeh, J. Hebling, et. al.. "Efficient terahertz generation by optical rectification at 1035 *nm*". *Opt. Express*, 15, 11706-11713 (2007).

34. L. Pálfalvi, J. Hebling, J. Kuhl, et. al.. "Temperature dependence of the absorption and refraction of Mg-doped congruent and stoichiometric $LiNbO_3$ in the THz range". *J. Appl. Phys.*, 97, 123505 (2005).

35. S. Sasamoto, J. Hirohashi, and S. Ashihara. "Polaron dynamics in lithium niobate upon femtosecond pulse irradiation:Influence of magnesium doping and stoichiometry control". *J. Appl. Phys.*, 105, 083102 (2009).

36. Y. Qiu, K.B. Ucer, and R.T. Williams. "Formation time of a small electron polaron in $LiNbO_3$: measurements and interpretation". *Phys. Stat. Sol.* (*c*)*,* 2, 232-235 (2005).

37. N. W. Ashcroft and N. D. Mermin. *Solid State Physics*. Saunders College, Philadelphia (1976).

38. V. N. Abakumov, V. I. Perel, I. N. Yassievich. *Nonradiative Recombination in Semiconductors*. North-Holland (1991).

39. J. Shan, F. Wang, E. Knoesel, et. al.. "Measurement of the Frequency-Dependent Conductivity in Sapphire". *Phys. Rev. Lett.*, 90, 247401 (2003).

40. M.C. Beard, G.M. Turner, and C.A. Schmuttenmaer. "Transient photoconductivity in GaAs as measured by time-resolved terahertz spectroscopy". *Phys. Rev. B*, 62, 15764-15777 (2000).

41. N. S. Stepanov. "Dielectric constant of unsteady plasma". *Sov. Radiophys. Quantum Electron*., 19, 683-689 (1976).

42. M.I. Bakunov, S.B. Bodrov, and M.V. Tsarev. "Terahertz emission from a laser pulse with tilted front: Phase-matching versus Čerenkov effect". *J. Appl. Phys.*, 104, 073105 (2008).

43. M. Clerici, M. Peccianti, B. E. Schmidt, et. al.. "Scaling mechanism for efficient wavelength conversion in laser plasmas". *Phys. Rev. Lett*., 110, 253901 (2013).

44. K. Y. Kim, J. H. Glownia, A. J. Taylor, et. al.. "High-power broadband terahertz generation via two-color photoionization in gases". *Opt. Express,* 15, 4577 (2007).

45. P. E. Ciddor. "Refractive index of air: new equations for the visible and near infrared". *Appl. Optics,* 35, 1566 (1996).

46. G. Rodriguez and G. L. Dakovski. "Scaling behavior of ultrafast two-color terahertz generation in plasma gas targets: energy and pressure dependence". *Opt. Express,* 18, 15130 (2010).

47. A. Couairon, and A. Mysyrowicz. "Femtosecond filamentation in transparent media". *Phys. Rep.*, 441, 47–189 (2007).

48. I. A. Kossyi, A. Yu. Kostinsky, A. A. Matveyev, et. al.. "Kinetic scheme of the non-equilibrium discharge in nitrogen-oxygen mixtures". *Plasma Sources Sci. Technol.,* 1, 207–220 (1992).

49. N. L. Aleksandrov, S. V. Kindysheva, M. M. Nudnova, et. al.. "Mechanism of ultra-fast heating in a non-equilibrium weakly ionized air discharge plasma in high electric fields". *J. Phys. D Appl. Phys.,* 43, 255201 (2010).

50. N. A. Dyatko, I. V. Kochetov, A. P. Napartovich, et. al.. "EEDF: the software package for calculations of the electron energy distribution function in gas mixtures". *http://www.lxcat.laplace.univ-tlse.fr/software/EEDF/*

51. Z. Q. Hao, J. Zhang, Y. T. Li, et. al.. "Prolongation of the fluorescence lifetime of plasma channels in air induced by femtosecond laser pulses". *Appl. Phys. B*, 80, 627-630 (2005).

52. G. Méjean, R. Ackermann, J. Kasparian, et. al.. "Improved laser triggering and guiding of meqavolt discharges with dual fs-ns pulses". *Appl. Phys. Lett*., 88, 021101 (2006).

53. J. Zhonggang, Z. Jiabin,W. Zhanxin, et. al.. "Low resistance and long lifetime plasma channel generated by filamentation of femtosecond laser pulses in air". *Plasma Sci. Technol.*, 12, 295-299 (2010).

54. X.-L. Liu, X. Lu, J.-L. Ma, et. al.. "Long lifetime air plasma channel generated by femtosecond laser pulse sequence". *Opt. Express*, 20, 5968 (2012).

55. J. Zhu, Z. Ji, Y. Deng, et. al.. "Long lifetime plasma channel in air generated by multiple femtosecond laser pulses and an external electrical field". *Opt. Express*, 14, 4915 (2006).

56. D. R. Bates, A. E. Kingston, and R. W. P. McWhirter. Proc. R. Soc. A 267, 297 (1962).